Net Shape HIPping of a Ni-superalloy: a study of the influence of an as-leached surface on mechanical properties

E. Bassini[(a,*)], L. Iannucci[(a)] , M. Lombardi[(a)], S. Biamino[(a,b)], D. Ugues[(a,b)], G. Vallillo[(c)], B. Picqué[(d)]

(a) Department of Applied Science and Technology (DISAT), Corso Duca degli Abruzzi 24, 10129 Torino, Italy.
(b) Consorzio Interuniversitario Nazionale per la Scienza e Tecnologia dei Materiali (INSTM), Via G. Giusti 9, 50121, Firenze, Italy
(c) *Avio Aero, Engineering Materials and Processes, Via I Maggio, 99 10040 Rivalta di Torino (TO), Italy*
(d) AUBERT & DUVAL – Pamiers Business & Development manager NNS & NS Parts Powder Metallurgy 75, bd de la Libération - B.P. 173 09102 Pamiers CEDEX – FRANCE

Abstract

Hot Isostatic Pressing (HIP) is a net-shape powder metallurgy technique where powders densification is achieved through the application of high temperature and pressure at the same time. Powders are allocated into a hollow steel mold called capsule or canister which gives the final shape to the particles. This technique is particularly useful for manufacturing complex components made of materials which are extremely difficult to process via forging or casting. Thus, HIP is particularly indicated to handle superalloy powders such as Astroloy, which is the object of the following study. One of the most attractive peculiarities of HIP is the low material waste obtained since the overstock is limited to the layers immediately beneath the steel capsule. At the end of the HIP cycle, the canister is typically removed using an acid leaching bath which is responsible for the alteration of the outermost layers of the final product. Only a little number of research papers deal with the optimization of the removal of these layers; Consequently, manufacturers often apply a very conservative approach by eliminating more material than is actually needed with a final machining procedure. This paper aims to optimize this procedure by systematically assessing the total thickness of the altered layer of material deriving from the HIPping and leaching process together. To achieve this goal, a set of samples were prepared by removing progressively thicker layers of material and then they were bend tested. Finally, the recorded mechanical properties were compared with those obtained with the samples machined from the core material. One of the main findings is that the removal of 500 µm of material is enough to recover mechanical properties which are comparable with those observed in samples coming from the core. More specifically, by eliminating the first 100 µm material, all the corroded layer is removed, which results in an overall increase of all the mechanical properties except for ductility. This property strongly depends on the number of prior particle boundaries arising from the HIPping process itself. Thus, the correct amount of overstock material must include both these layers.

Keywords

Astroloy, HIPping, Powder Metallurgy, Near Net Shape, Acid Leaching

1 Introduction

In the last decades, the aeronautical industry has been engaged in the research of new materials and process routes to produce components which can function in more challenging working conditions. An interesting field is represented by materials used in turbine engines, where one of the main purposes is to reach high temperatures to increase the efficiency of thermodynamic cycles, as reported in Reed, (2006). A feasible solution has been found in Nickel superalloys, which can guarantee a unique combination of high-temperature strength, toughness, and resistance to degradation in corrosive or oxidizing environments, as

demonstrated in the work of M. J. Donachie, (2002). According to this, considering the low-pressure-turbine stage, Ni-grade alloys such as Waspaloy or Inconel 718 may no longer be suitable and different alloys must be used, as published in the review developed by Rolls-Royce, (1996). In particular, the presence of alloying elements like Titanium and Aluminum, which are involved in the formation of γ' precipitates Ni_3(Al, Ti), induces the high mechanical strength and high-temperature resistance of Ni-superalloys. (M. J. Donachie and Donachie, 2002) demonstrated how, due to the higher amount of γ', Ni-grades like Astroloy become eligible for this application as confirmed by Geddes et al., (2010)**.** Astroloy was initially intended for the wrought route but, due to its high alloying element content, which enhances the γ' precipitation, the material was practically unforgeable. The principal reason for this limitation was the very narrow forging temperature range which was further narrowed by the chemical segregation of the ingot. Forging was therefore, not the most eligible manufacturing route for Astroloy, especially because it is extremely complicated and characterized by high material waste. The problem was subsequently overcome through the powder metallurgy route, which allowed the use of Astroloy, especially in gas turbine engines and turbine disks. Astoloy powders can also be hot extruded as described by Popoolaa (Popoolaa et al., 2016). Other researchers like (Wisniewski and Beddoes, 2009) used hot extrusion followed by isothermal forging to process Astroloy. In their work, (Baccino et al., 2000), evidenced how the powder metallurgy route, in particular, the Hot Isostatic Pressing (HIPping) was a feasible way to process Ni-superalloy components with a complex shape. As described in the work of (Gessinger, 1984) and more recently also by (Hjorth, 2007), HIP consists of the filling of a steel capsule (used as a mold) with superalloy powders, which is sealed to create a vacuum. The subsequent application of high temperatures and pressures cause the powders to densify. Pressure is applied using an inert gas, so the capsule that already has the final shape of the component undergoes an almost uniform shrinkage. A general overview of HIPping can be found in the published work from (Atkinson, H.V., and Davies, S., 2000) and (Broeckmann, 2012). More specifically, (Bampton et al., 2005) worked in the HIP field describing the fabrication of rockets made with Ni superalloys. (E. Bassini et al., 2017a), on the other hand, worked specifically on HIPped Astroloy studying its heat treatment in depth. According to the authors knowledge, currently, Hot Isostatic Pressing is the standard manufacturing route for Astroloy due to the appeal of its net-shape aspect. Other researchers are trying to further improve this process by adding a part of the heat treatment during the HIP cycle itself by employing the HIP-quench technique which allows the elimination of the solutioning heat treatment (Bergmann, 1990), as discussed more recently by Eklund in (Eklund and Ahlfors, 2018). At the end of the HIP process, the steel capsule is eliminated through acid leaching to obtain the final product. In their work on Astroloy (E. Bassini et al., 2017b), described how, during the soaking in the HIPping chamber, diffusion processes take place between the steel and the superalloy powders, so the composition of the first layers of the component are altered and they must be removed by machining. Other authors also described the problem of the contamination of the interlayer between the capsule and the processed superalloy but for different alloys. For example, (Go and Echeberria, 2003) studied the diffusion between a steel capsule and the Sanicro 28, while (López et al., 1996) focused on steel cladded to IN625. Another example is found in the research work by (Qiu et al., 2013) who studied the diffusion between Steel and Hastelloy G3. In addition, some researchers, who worked on Titanium alloys such as (Davidson et al., 2006)**,** and more recently (Zhang et al., 2010) underlined the complexity of the final machining used to remove the external surface of the components contaminated after HIPping. In the literature, it was also found that some researchers used a glass capsule to hip AISI 316L and other superalloy powders, i.e. (ElRakayby and Kim, 2018) demonstrating how glass leads to more uniform compaction of the powders concerning traditional steel capsules, even though a description of powder-glass interface evolution was not given. They also affirm that capsule removal is faster and cheaper. Despite this, the majority of works dealing with the HIP of superalloy powders involve the use of a steel capsule.

This study will assess the alterations produced at the interface between Astroloy powders and a low carbon steel capsule during HIPping and the damages caused by the corrosion during the acid leaching. It further aims to quantitatively identify the correct amount of overstock that must be removed from the surface, after the acid leaching, to reach the optimal mechanical properties.

2 Material and methods

2.1 Material and sample preparation

The Astroloy powders, consisting in particles with an average size of 70 µm and maximum diameters of 106 µm, was employed for the realization of HIPped square section bar (100x100x1000 mm^3) according to the production cycle described in (Raisson, 2008; Raisson et al., 2011). After that, a heat treatment was performed on the material: it consisted in a solutioning treatment at 1115°C for 4h and then an aging at 760°C for 8h both performed into a low-pressure furnace TAV MINIJET HP S/N 235. **Table 1** shows the composition of the commercial Astroloy grade powder used during this work, expressed in wt%. The composition of the alloy was evaluated via plasma emission spectrometry with an Atomic Emission Spectrometer SP12 model TJA Iris Advantage Radial. Oxygen and Nitrogen were analyzed with melting under inert gas using a LECO TC436AR analyzer. Carbon and Sulphur were assessed through infrared absorption analysis using a Leco CS744. The mild-steel capsule composition before HIP according to its datasheet is also reported.

Table 1 Chemical composition of Astroloy base material

Material:	Ni	Co	Cr	Mo	Al	Ti	Fe	Zr	N	C	S	O
Astroloy [wt%]	Bal.	17.8	14.3	5.6	4.6	3.7	0.2	0.05	0.004	0.014	<0.002	0.01
Capsule [wt%]	-	-	-	-	-	-	bal.	-	-	0.16	0.040	-

The specimens (8x7x40 mm^3) illustrated in **Figure 1** were cut from Astroloy bar to have one side still covered by the steel capsule (about 3 mm thick).

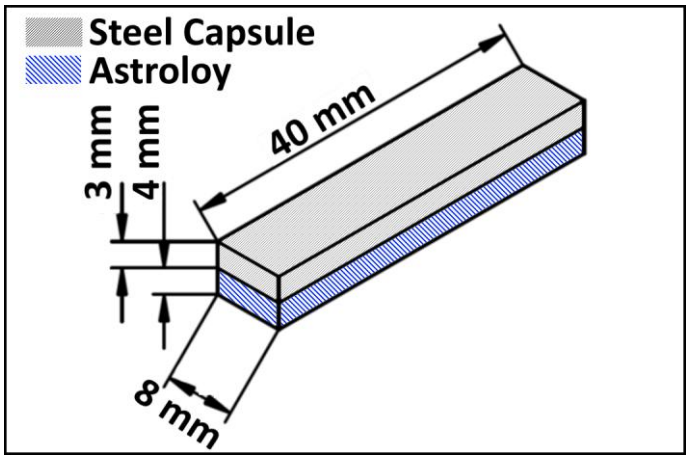

Figure 1 Drawing of the specimen before the acid pickling process

2.2 Acid Leaching and mechanical characterization of the samples

The leaching process was performed using a solution containing 5% HNO_3 and 5% HF in distilled water. Samples, which have only one side covered by the steel capsule, were dipped into the leaching bath, with the steel downward. Specimens lean on special supports which limit the contact surface between the two (see **Figure 2**); thus, corrosion products were able to fall, avoiding to accumulate and therefore, without slowing down the kinetics of the process. Samples were sunk in the acid bath for 24 hours to eradicate the steel capsule.

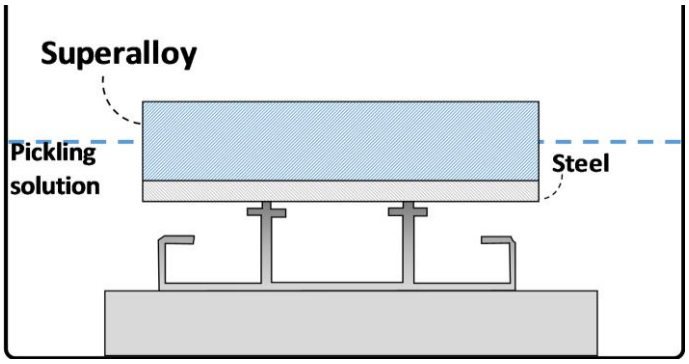

Figure 2 Drawing of the apparatus for the acid pickling process (pickling bath, supports, and sample)

The layer of material altered by HIPping and leaching processes must be removed and its final thickness was identified performing several bending tests with samples from which progressively thicker layers of material were machined away.

At the same time, three samples were machined from the core of the bar to have a reference level for the mechanical properties investigated. All samples for bending tests prepared in different ways were 8x4x40 mm and for each set, three identical specimens were employed.

Firstly, bending tests were performed on as-leached samples which have a surface roughness (R_a and R_z) of 4.84 ± 0.41 and 21.93 ± 0.68 respectively. In addition, to evaluate the effect of roughness caused by the acid leaching, some samples were tested after grinding the leached surface using a 1200 grit SiC paper removing a negligible amount of material. These samples were referred to as "ground" and are characterized by a slightly lower roughness, i.e., 4.32 ± 0.31 (R_a) and 18.22 ±0.86 (R_z). Other samples were obtained via machining, removing a fixed and increasing amount of material, i.e., removing a thickness of 50, 100 or 500 µm below the leached surface. The material was removed using an automatic polishing machine Presi Mecatech 234 whose samples holder was modified in order to accommodate the sample of Figure 1.This test rig allowed to apply the pressure with the pistons evenly onto the samples, ensuring flat surfaces. The progressive material removal was monitored using two Johansson ceramic reference blocks of different height positioned on the left and right side of the samples respectively. The difference in height among reference blocks and samples were measured at the beginning (prior to machining) and after each grinding step with the contact profilometer Mahr Marsurf CD120. The procedure was repeated until the target amount of material is removed. The differences in height were measured in 5 fixed positions in order to verify the planarity of the sample surface. Samples were prepared using an 800 grit SiC paper obtaining a final roughness of 0.3 µm (R_a). The progressive removal of material produced different starting conditions for the bending tests, as highlighted in **Figure 3**.

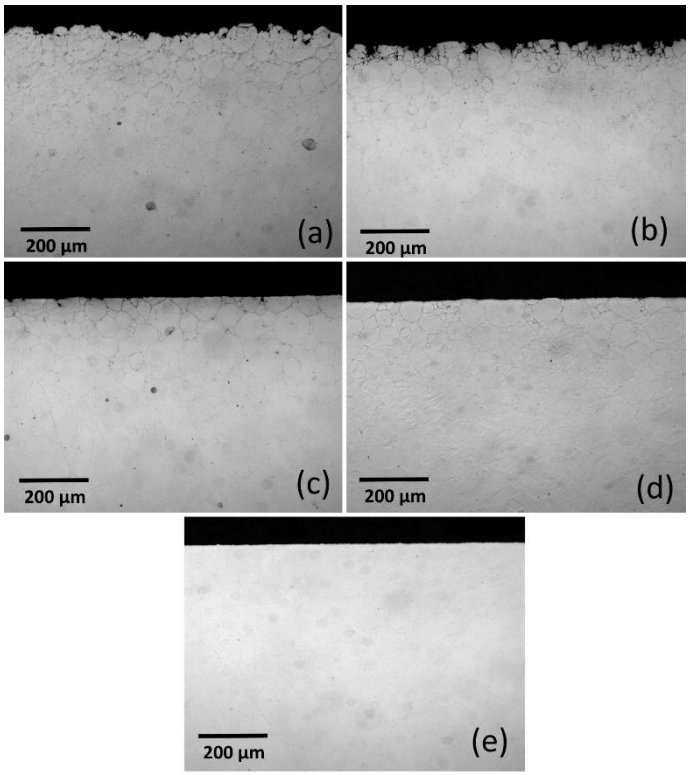

Figure 3 Optical micrographs of different samples after polishing with colloidal silica: a) As-leached; b) ground; c) 50 µm removed; d) 100 µm removed; e) 500 µm removed

Three-point bending tests were performed using a ZWICK Z100 machine with hydraulic control. The load cell could reach 100 kN and the force was applied by the movement of the crosshead with a speed of 1 mm/min. The standard followed was ASTM E290-97a 'Standard Test Methods for Bend Testing of Material for Ductility' ("ASTM E290-14" 2014). All tests were carried out at room temperature. Specimens were located on the supports with the as-leached surface downward, to load it in tension.

2.3 Microstructural and roughness characterization

Assessment of as-leached surface was performed by optical and electron microscopy. Starting from lower magnification, a stereomicroscope Leica MS5 was used to characterize the morphology of the samples after acid leaching in top view. Furthermore, the cross section of leached and bending samples was observed with light Optical microscope Leica Mef4 after being mounted in thermosetting resin, metallography prepared by grinding up to 2400 grit and polished using diamonded paste down to 1 µm. Scanning Electron Microscope (SEM) MEB Leo 1450 VP was used to characterize the as-leached surface and to analyze the fracture surfaces after bending tests.

Compositional analysis was performed using Energy Dispersive Spectroscopy (EDS) detector Oxford Instrument ISIS Link Pentafet 7353 working in conjunction with the SEM. EDS analysis was used to assess the diffusion of elements due to the HIPping process. EDS was performed on samples cross sections for a total depth of 80 µm using spot analysis with a distance between two consecutive points of ca. 10 µm. Elements measured across the interface are Al, Ti, Cr, Fe, Co, Ni, and Mo.

Finally, roughness measurements were performed with a Hommelwerke Tester T1000.

3 Results

In this section, a characterization of the material after acid leaching will be provided. Firstly, the effect of the acid pickling on outer layers of material will be analyzed; then its influence on mechanical properties will be studied.

3.1 Microstructural assessment of as-leached surface

Samples after the leaching process were observed to investigate the morphology of the as-leached surface and to check if capsule residues were present.

As will be discussed later in detail, the as-leached surface shows a morphology which is reminiscent of the raw powder material used during HIP. **Figure 4** shows Astroloy powders at low magnification. As can be seen, particles are almost exclusively spherical and with different size. Even though the particle size distribution is quite broad, the average powder size is 70 µm.

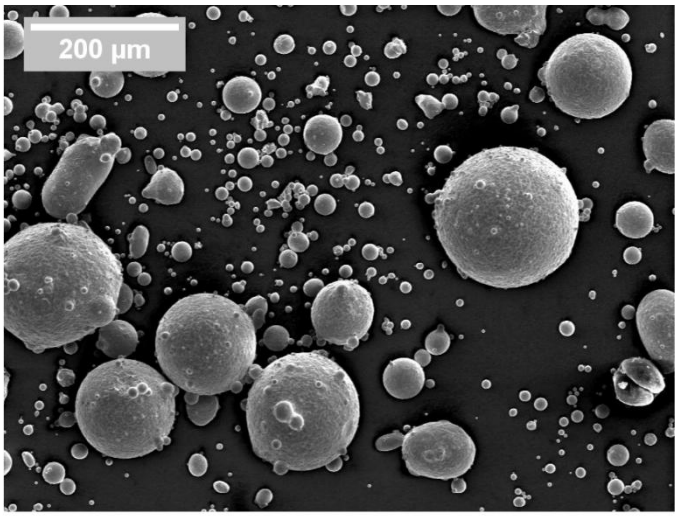

Figure 4: Astroloy powders used during HIP observed with FESEM

As can be seen in **Figure 5 a)** and **b)**, the surface is irregular and at higher magnifications, it is possible to recognize bumps easily. The bump dimensions were measured and range between 73 and 100 µm, and thus, their diameters are compatible with those of superalloy particles, confirming that particles profiles are preserved. The residual profile of superalloy powders is present on the as-leached surface of HIPped samples because, as already reported in other studies about HIPped Ti6Al4V (Cai et al., 2016) or earlier by (Davidson et al., 2006), during the HIPping process the steel capsule is indented by the first layers of powder, which indeed, are not deformed. EDS maps were taken on the as-leached surface as shown in **Figure 5 c)**. The maps evidence several carbides rich in Ti or Mo embedded in a Ni matrix. Iron is present since, during HIP, it diffused towards the powders, but no agglomerates were found, indicating that the capsule was adequately removed from all the samples. The squared voids shown in the insert of Figure 5 b) and more clearly in Figure 5 c) are formed because the leaching bath, similarly to Kalling solution, consumes the γ' intermetallic more easily than γ matrix leaving the characteristic cubical cavities.

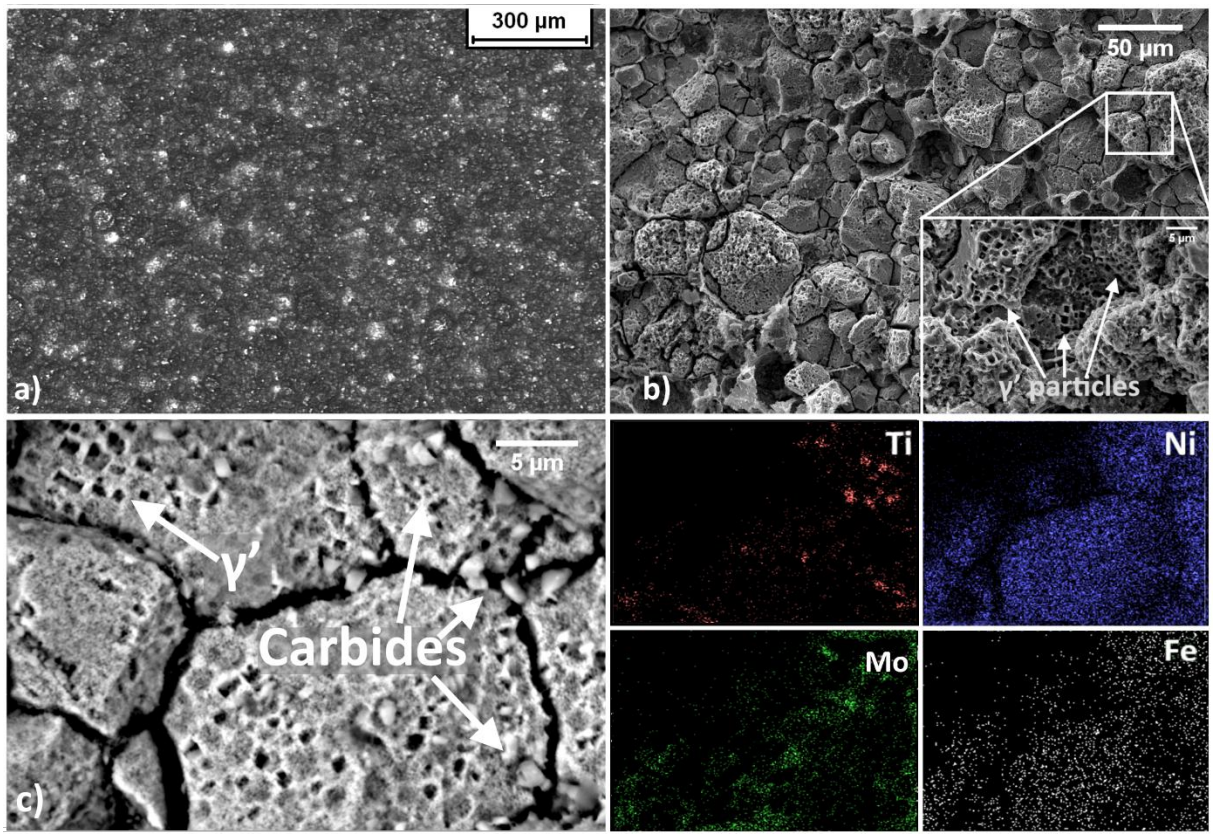

Figure 5 Leached surface of Astroloy observed with Optical Stereo Microscope a) and with SEM b). EDS Maps showing Ti, Ni, Mo, and Fe distribution c).

To better understand which layers were removed by the acid leaching, a cross-section of the as-HIPped interface is shown in **Figure 6 a).** The morphological and compositional features indicate that the steel capsule is present in the upper part of the sample. More specifically, the first part is ferritic, which can be demonstrated considering the meager amount of alloying elements (EDS shows more than 95% of Iron) and the morphological aspect, consisting of an over-etched phase, due to the feeble resistance of ferrite towards etchants. On the other hand, Figure 6 b) shows the layer below the Ferritic strip. This part of the interface is characterized by a higher content of Cr and Ni, and own an acicular morphology, which is compliant with a low carbon martensite. Below the martensite, due to the intense migration of Ni and Cr from the superalloy towards the steel capsule, a transition layer is formed. In this layer, the material, due to its composition, is more similar to an austenitic stainless steel, even though, its corrosion resistance properties are practically unknown. In deeper layers, it is possible to recognize the external surfaces of Astroloy powders, indeed, the Prior Particle Boundaries (PPBs) (Aubin et al., 1980), and grain boundaries, indicated in **Figure 6 a)** with a dotted line and with arrows, respectively. Finally, **Figure 6**_c) shows, in greater detail, the coarse carbides located at the ICP.

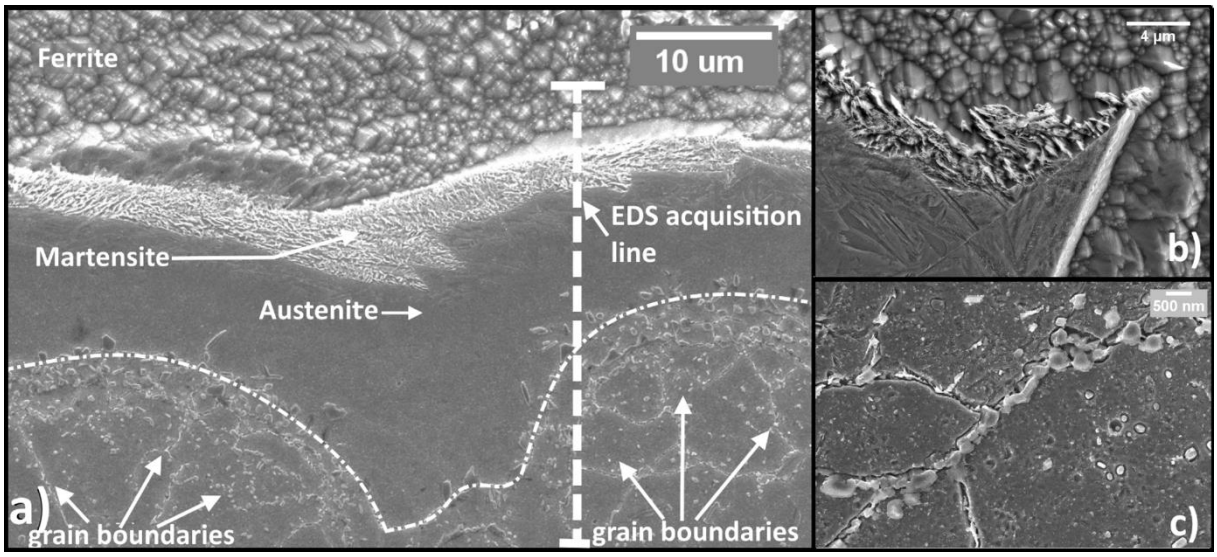

Figure 6 Appearance of the as-HIPped capsule-Astroloy interface after etching with Glyceregia observed with SEM a), a detail of the acicular phase found below the ferritic strip, compliant with a low carbon martensite b) and a detail of carbides in the ICP zone c).

On the other hand, Figure 7 shows the compositional gradient of elements in the cross section for Fe, Ni, Cr, Mo, Ti and Al assessed via EDS along the white dashed line in Figure 6 a).In particular, in the EDS plot, a strong increase in Ti amount is recorded and highlighted with a red circle in the proximity of the PPBs. This fluctuation is due to a strong precipitation of Ti carbides, that occurs in the area called "intense carbide precipitation zone" (ICP), corresponding to the original contact surface between the capsule and the superalloy (E. Bassini et al., 2017b). These coarse carbides were also observable in **Figure 5 c)**. Moreover, the layers just below the ICP are characterized by a chemical composition notably different from that of the nominal Astroloy and remarkably similar to a Fe-Ni superalloy. These Fe-rich layers are a consequence of the Iron diffusion from the steel capsule to superalloy samples during the HIPping stage. For completeness, all the other constituting phases are described in depth in a previous study (E. Bassini et al., 2017b).

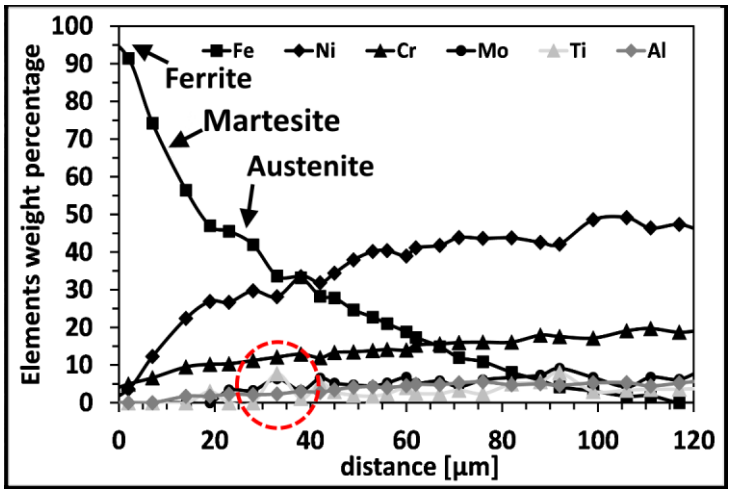

Figure 7: EDS showing compositional gradient located at the interface between Steel capsule and Astroloy surface.

Figure 8 a) and **b)** show the outermost layer of an as-leached sample in cross-section. Several phases can be identified below the corroded layer thanks to the backscattered detector and the EDS maps. Despite ca. 20 µm of material is severely damaged by the acid leaching, the contour of the powders is still entirely recognizable. The powder boundaries are evidenced by the presence of a carbide network whose composition is highlighted in the EDS maps of **Figure 8 b)**. Carbides located at powders boundaries and those which precipitated within them are all Titanium rich carbides, as also confirmed observing the maps for Mo and Cr which appear to be well dispersed through the γ matrix.

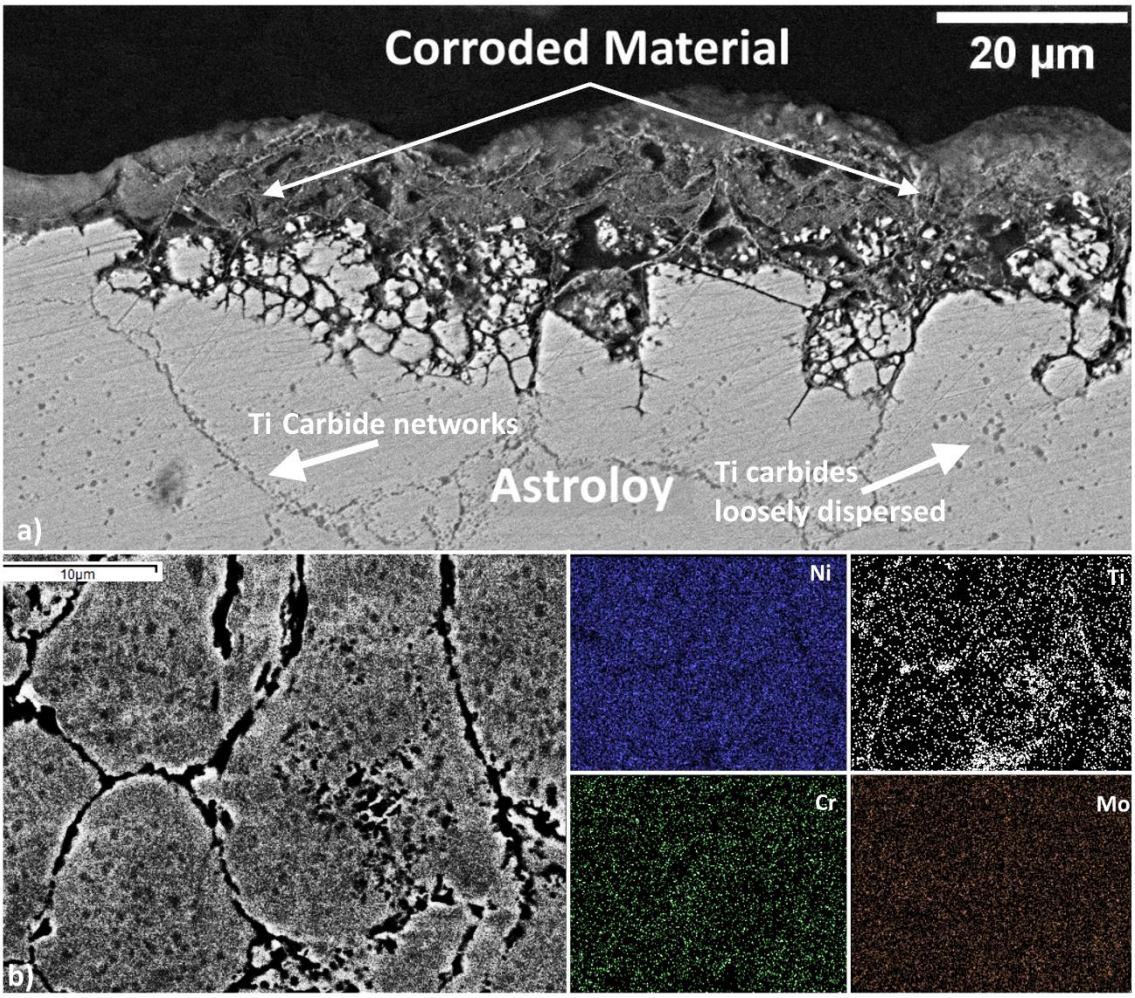

Figure 8 Electron scanning micrographs with secondary electrons of the cross-section of the sample after acid pickling. Signs of corrosion are evident on the first layers of particles a). EDS maps showing Ti carbides visible inside and at the powder boundaries.

The acid pickling process caused extensive corrosion of the outmost layers of the superalloy and this led to severe damage to the material. The two preferential paths of the attack were PPBs and grain boundaries. Some particles retained their spherical shape even if partially deteriorated; in other cases, particles were detached entirely and only voids are observable. The presence of such severe corrosive attack can be attributed to two main reasons. Firstly, the presence, although limited, of nitric acid in the pickling bath, which is aggressive also towards Astroloy as can be found in (Friend, 1980) or in (Adler et al., 2003). Secondly, the existence of a diffusion layer in the first hundreds of micrometers, having a lower resistance to chemicals. As already observed in other research works dealing withTi6Al4V (Scherillo et al., 2015) and Astroloy (E. Bassini et al., 2017b), during HIPping, iron and carbon atoms diffuse to the superalloy side while the steel enriches in nickel and chromium. The interface, although well visible in optical micrographs, has a very smooth compositional gradient and for this reason, the difference in corrosion resistance of single layers is not enough marked to stop deterioration in a clear way. Surface roughness was measured and R_a ranged between 4.43 and 5.25 µm, in good agreement with those estimated in (E. Bassini et al., 2017b) where the values were calculated via an image analysis software, only observing the interface in cross-section, without performing the real leaching experiment. Roughness values here found are also in good agreement with those found in the literature for HIPped Ti6AlV4 (Davidson et al., 2006) and later by (Zhang et al., 2010). Observing **Figure 8 a),** it is evident that the leaching process removed a layer of material, so it is necessary to evaluate its thickness. The amount of removed material is assessed through the comparison of 50 pictures (for a total investigation length of 5 mm) showing the as-leached interface in the cross-section with those of the as-HIPped material. All the figures indicate that the process stopped in the layers

immediately below the intense carbide precipitation zone. As also suggested in (E. Bassini et al., 2017b) it can be stated that acid leaching completely removed the martensitic band.

Furthermore, the austenitic band was almost entirely dissolved and only small portions are still barely recognizable. On the other hand, the intense carbide precipitation zone and the Fe-Ni superalloy band are well visible; even though the corrosive process strongly alters them. Thus, it can be concluded that the acid leaching removed the steel capsule and a portion of the diffusive layer whose thickness ranges between 30 and 35 µm, or in other words, all the layers on the left side of the red circle of **Figure 7**.

3.2 Mechanical properties assessment

In order to quantify the amount of overstock that must be removed from the surface of HIPped materials, different kinds of samples were prepared for the bending testing. Each sample has the surface subjected to tensile in a state that was representative of different specific preparations: as-leached, slightly ground, 50 µm, 100 µm, 500 µm and core (the 50 to 500 µm identifying code refers to the thickness of the material progressively removed starting from the as-leached surface, whereas the core id. code refers to samples removed roughly at mid-section of the hot isostatically pressed billet). The results of bending tests are listed in **Table 2**. Due to industrial secrecy policy, the mechanical levels recorded for samples with as leached surface and progressively increasing surface layers removal are given not as absolute values, but as percentages of the values recorded by samples removed from the core material, used as reference. Actually, the so-called core samples can be classified as samples from which the amount of material removed is so high that the surface subjected to tensile stresses can be considered as not altered from the capsule removal procedure and thus to be representative of the bulk material properties.

Table 2 Variation of mechanical properties concerning the amount of removed material

Sample	Amount of removed material [µm]	σ_γ bending	Bend Strength	dL at break
As-leached	0	91 ± 4.5	78 ± 4.6	73 ± 0.5
Ground	≈5	96 ± 4.7	86 ± 4.8	75 ± 0.7
50 µm	50	98 ± 0.7	91 ± 1.2	75 ± 0.9
100 µm	100	99 ± 0.8	96 ± 1.3	75 ± 0.7
500 µm	500	99 ± 0.7	98 ± 0.8	98 ± 0.3
Core material	n.a.	100	100	100

Figure 9 a), **b)** and **c)** show the yield strength, the ultimate bending strength and elongation at break, respectively, plotted as a function of the thickness of removed material (starting from the as-leached surface).

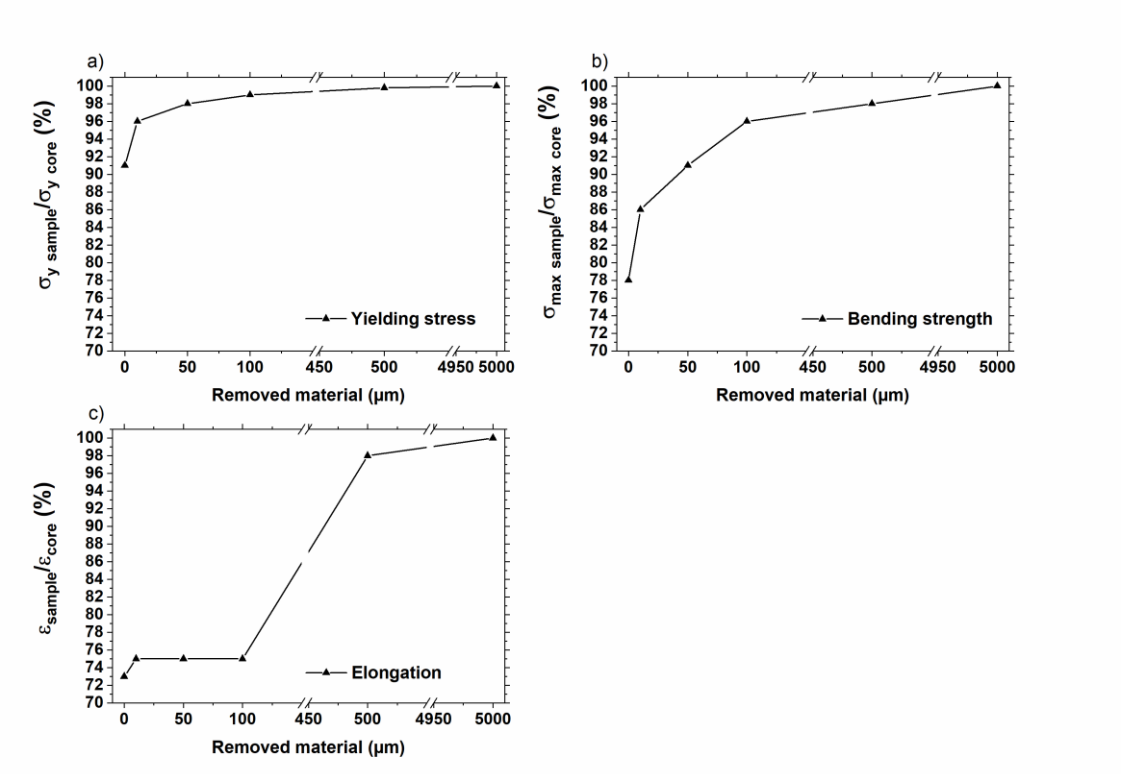

Figure 9 Mechanical properties a), b) and elongation c) after bending tests (data are expressed according to the ultimate bending stress and elongation measured on samples coming from the material core)

It is noteworthy that yield and bending strengths show a continuous variation that approaches asymptotically the core values. In particular, it is important to underline that the yield strength achieves the asymptotic core level within a shallow layer from the surface, i.e. between 100 and 500 µm of removed material. On the other hand, the maximum bending strength recovers the core property level within a higher distance from the surface, through a progressive moderately increasing behavior. Finally, the elongation to break behavior as a function of the amount of material removed from surface has a pronounced step again between 100 and 500 µm of removed material.

These different mechanical properties can be explained by considering the specific microstructural features present in the different layers by moving from the as-leached layer to the deeper layers and further to the core. The external layers of the as acid leached and slightly ground surface are affected by microcracks and grain boundaries decohesions, deriving from the corrosive attack procedure. Even in slightly ground samples some residual of grains decohesion are detectable. These features are responsible for the depression of all mechanical properties. More specifically, in this condition, Astroloy specimens show the lowest yield and ultimate bending stresses (respectively -10 and -22.5 % with respect to the unaltered material). Moreover, ductility is lowered by a -26% with respect to the core material. By removing these two outer layers the surface that is subjected to tension is representative of deeper layers of the material. At such levels, the microcracks and grain boundaries decohesion are not more visible, however the spherical profile of prior particle boundary is clearly detectable. The fact that such profile is very evident is due to the particular decoration of carbides and other precipitates located along it. Such precipitates are partially the so-called PPBs (oxides and carbides already present on the surface of the powder) and partially carbides formed during consolidation through solid state diffusion of carbide forming elements from the core of the particles towards their shell. The fact that prior powder particles remain unaltered in shape is due to the fact that on this outer shell of the consolidated material the locally applied conditions of pressure and temperature favor consolidation by only solid-state diffusion rather than by combined plastic deformation and diffusion. As far as the other microstructural features are concerned, very fine and spherical gamma prime particles were found to precipitate within the grains at this location (E Bassini et al.,

2017). Actually, the traditional fine and cuboidal gamma prime formation was observed only in deeper regions, i.e. below 100 µm from the as leached surface. This gradual modification of the gamma prime morphology when progressively moving from the external to the inner layers is consistent with the fact that the chemical composition changes throughout such layers. In particular, the iron content is high in the external layers as a consequence of solid diffusion from the capsule base material into the consolidating Ni-alloy. However, by considering deeper layers of the consolidated Ni-alloy the iron progressively reduces and achieve the typical low value of the average Astroloy chemical composition. Actually, iron is found in literature to promote such spherical morphology of gamma prime that is typical of Ni-Fe-Cr alloys.

According to these observation, one can explain the behavior of the different properties as reported in Figure 9. Ductility is dominated by the presence of brittle phases dispersed in the matrix. Within the first 100 µm the formation of these phases is particularly pronounced and results in coarse particles and clusters of finer particles located along the prior particles profile. Furthermore, the limited plastic deformation action at which powders were subjected during the HIP consolidation impedes their uniform dispersion into the matrix. As a consequence, as far as the microstructure is dominated by these features the maximum deformation prior failure is highly limited. Between 100 and 500 µm such microstructural feature progressively disappears and thus it does not dominate the failure mode. Therefore, the maximum macroscopic deformation prior to failure increases.

As far as the yield strength in bending condition is concerned this is rather dominated by the presence of gamma prime within grains. These are the microstructural features that impede dislocation movement and thus, increase the resistance of the material to plastically deform. Both gamma prime dimension and morphology influence the total yield strength of the material. Actually, the increase in gamma prime particles dimensions and the change from its morphology from spherical to cuboidal provides an increase in yield strength. Therefore, by increasing the material removal from the as leached surface, layers of materials with different gamma prime features are exposed and subjected to tension. This modulation of the gamma prime dimension and morphology is progressive and thus provide a progressive increase in yield strength as we stress always deeper layers of the HIP Astroloy.

Finally, the UBS is related to both the microstructural features discussed so far. On one hand, the improvement of gamma prime structures provides a higher capacity to accommodate plastic strain, thus leading to an increase of UTS as we test always deeper layers of the material. On the other hand, the presence of brittle phases at preferential patterns, especially along prior particles profiles, is a limitation of strain accommodation at these sites. Therefore, the macroscopic UBS is progressively increased as we test always deeper layers of the material, but the maximum stress that can be sustained by the material is also limited by the presence of coarse and brittle phases not uniformly dispersed into the matrix. As a consequence, the increase in UTS is progressive as we test deeper layers, but it achieves a stable saturation level with a lower rate. In other words, it is necessary to remove a higher amount of materials to recover the bulk Astroloy UTS and ductility. On the contrary, the Yield Strength of bulk Astroloy can be recovered with shallower material removal.

4 Discussion

4.1 Fractographic surfaces observation

SEM was used to examine the surfaces of broken samples and different behaviors were detected among them depending on the amount of removed material. **Figure 10 a-f** show a comparison, at the same magnifications, of fracture modality and aspect of the side in tension during the bending test, thus with the leached surface at the bottom, for all samples.

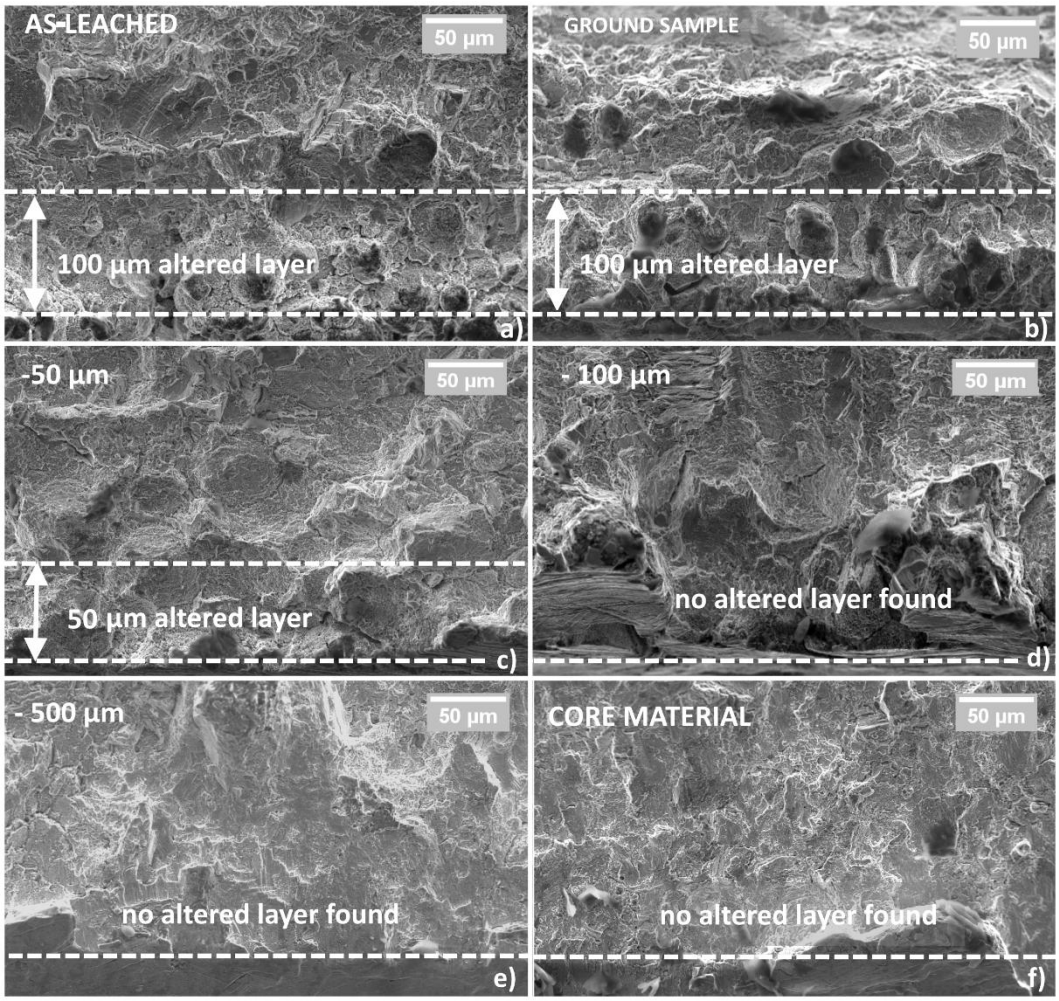

Figure 10 Fractographic surfaces of samples after bending tests taken with secondary electron SEM

In as-leached samples, it is possible to observe a 100 µm layer of corroded material ***indicated as 'altered layer'***, that led to a brittle fracture. Actually, it must be reminded that preferential paths, such as grain boundaries or prior particle boundaries, let dissolution takes place also in areas located under the surface of the sample see **Figure 10 a)** and **Figure 11**. Moreover, prior particle boundaries are clearly visible, and fracture is transgranular for the first 100-150 µm.

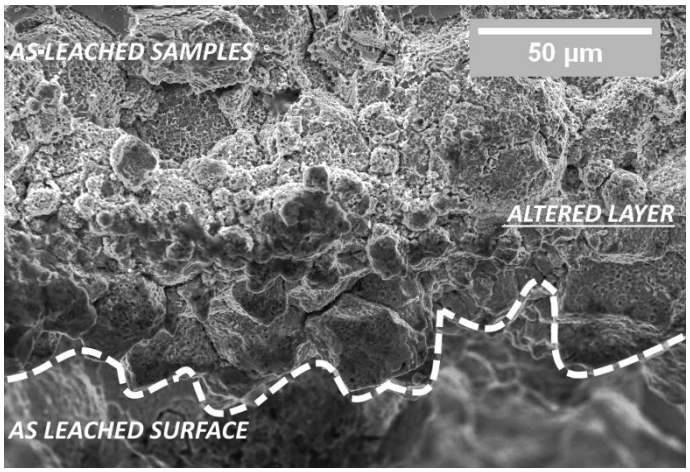

Figure 11 Fractographic surface after bending test showing corroded layer beneath the surface

Ground samples do not show significant differences from the as-leached ones since only a negligible amount of material was removed. The 100 µm brittle layer is still evident. The comparison of **Figure 10 c)**

and **d)**, shows that the layer characterized by brittle behavior is reduced to 50 µm in the first case and disappears in the latter. In this last case, no sign of corrosion is evident, but the fracture appearance is still brittle. Finally, in the 500 µm samples, neither corrosion nor intergranular fracture can be detected. In these specimens, the common fracture modality of Astroloy superalloy can be observed, which means that, although the material has a ductile behavior, sometimes cleavage planes can be found. Moreover, from a comparison of **Figure 10 e)** and **f)** it is possible to observe that the fracture surface of the 500 µm sample is practically indistinguishable with respect to that obtained with a sample coming from the core, as a confirmation that 500 µm is the correct overstock amount to be removed after leaching.

Further observations were made on broken specimens. In particular, in SEM micrographs it was noted that, besides the main crack that led to the failure of the samples, other secondary cracks were present on the surface in tension during the bending test (see **Figure 12**). Namely, secondary cracks were visible in all samples with the only exception of the 500 µm and core material specimens.

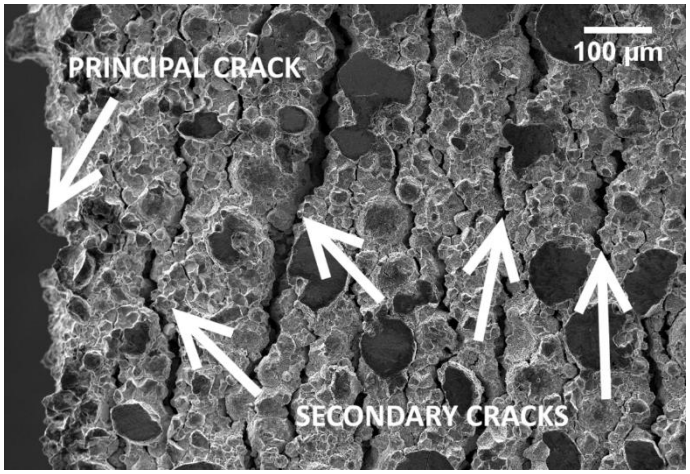

Figure 12 SEM micrograph showing, after the break, the surface in tension during the bending test

Thus, the presence and quantity of secondary cracks in the different kinds of samples were used as a mean to understand the capability of the material of withstanding the applied load as the finishing condition was changed. For this reason, specimens were cut into two halves following their axial direction and then one of the two surfaces was ground and polished (according to the representation of the sectioning plane of **Figure 13**).

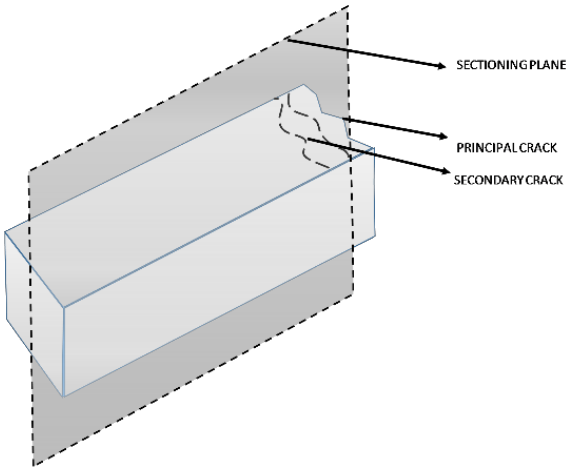

Figure 13 Drawing of the sectioning of samples for secondary cracks observations

At first sight, three main characteristics are modified by changing the amount of removed material: the number of formed cracks; the depth up to which cracks can travel into the material; the modification of sample curvature.

Figure 14, realized aligning the major crack of each sample at the right side of the picture, shows the first 3 mm of the surface from the fracture for all samples. Then, the distance separating the principal crack from the last visible secondary crack was measured, neglecting the curvature caused by the bending test. More specifically, for the following calculations, only grooves deeper than 60 µm, i.e., greater than the average particles diameter, were considered as secondary cracks.

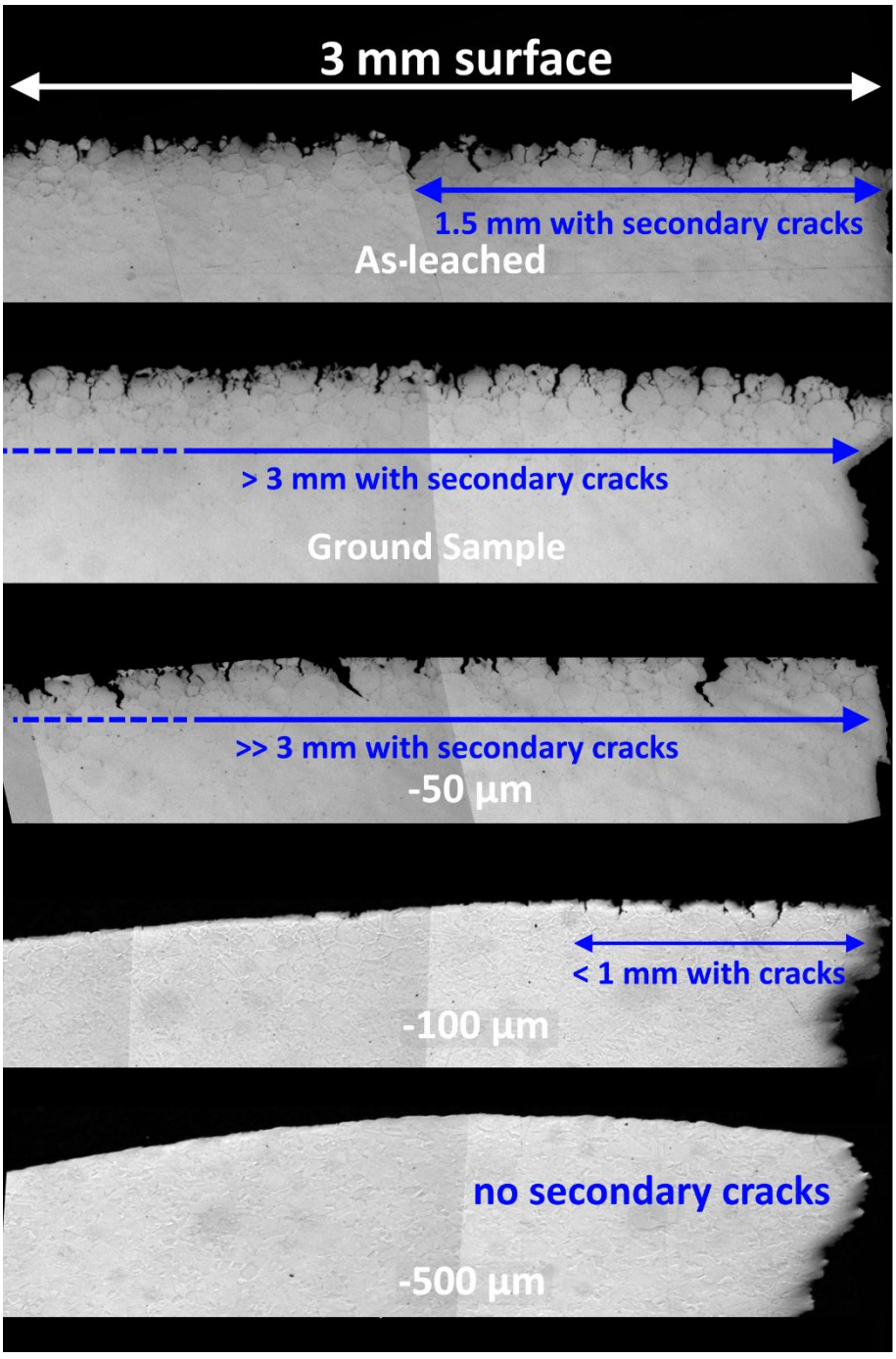

Figure 14 Optical micrographs of samples after bending test with progressive material removal from top to bottom (principal cracks is on the right side of the picture)

Results are resumed in **Figure 15 a)** and **b)**. As can be seen, the distance at which secondary cracks are visible increases passing from as-leached to 50 µm samples, resulting particularly evident for the ground and the 50 µm samples where last visible secondary cracks were far beyond the 3 mm of the investigated surface (see **Figure 14**). On the other hand, the surface covered by secondary cracks is sharply reduced in 100 µm and 500 µm specimens, being the latter utterly free of surface defects.

As a further examination, **Figure 15 b)** shows the distance covered by secondary cracks as a function of removed material for all samples, with a trend similar to the one of **Figure 15 a)**.

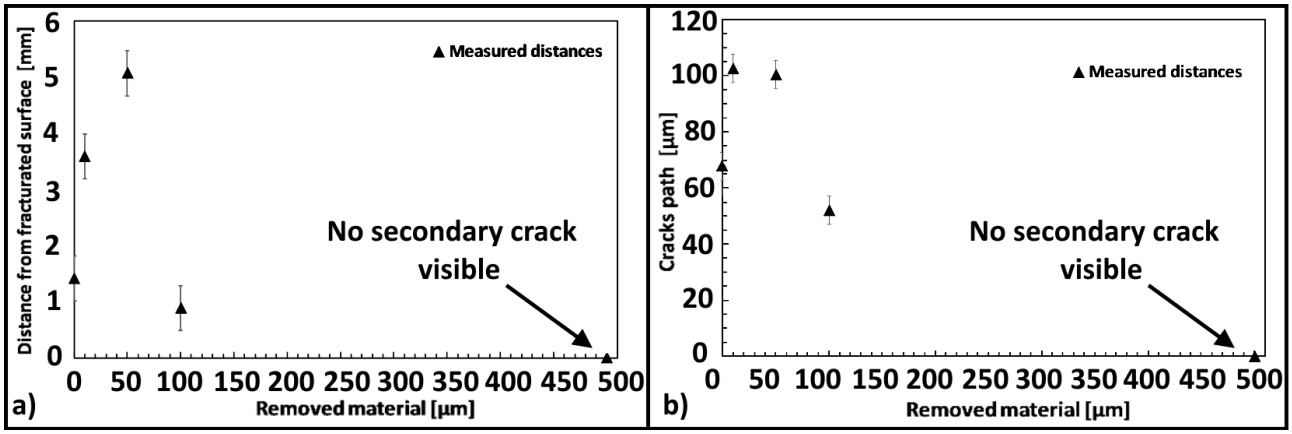

Figure 15 Plot of distance covered by secondary cracks in the samples as a function of removed material

From the collected data, it can be stated that material in as-leached conditions presents only one catastrophic defect. In the as-leached sample, first layers are so compromised that, once a critical flaw is formed, superalloy is not able to withstand other damages. Profile irregularities, coming from the leaching process, act as sites for stress concentration and cracking is favored.

Since the surface remains in traction only for the time necessary to originate the principal crack and having its full propagation from side to side, secondary cracks remain very limited in number and depth. By roughness reduction or removing material (up to 50-100 µm) less critical points remain at disposal for detrimental crack formation; thus the material can better withstand tensions.

During the propagation of the principal defect, tensions redistribute onto the surface. Since the material is very ductile, there is the probability that, around the principal defect, the applied stress overcomes grains binding strength, which is also lowered by the presence of PPBs. When these conditions are satisfied, grain debonding occurs and secondary cracks form and grow with easiness. After the nucleation, cracks propagate in the first 100 µm layer following PPBs and grain boundaries (intergranular fracture). The propagation is due to the PPBs presence that weakens grain boundaries, as exemplified in **Figure 16**.

It can be affirmed that favorite sites for secondary cracks nucleation are eliminated by removing more material. Moreover, the binding strength among grains is increased by the PPBs absence, leading to the disappearance of secondary cracks, which even do not nucleate in 500 µm samples.

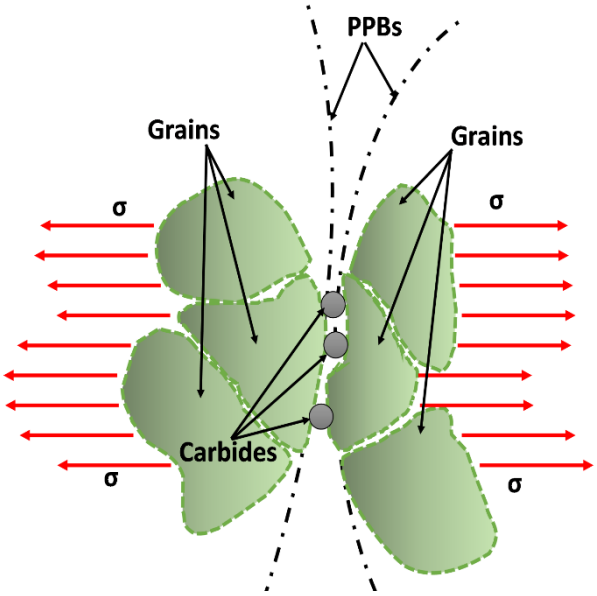

Figure 16 Sketch of the failure mode in the first layers of materials characterized by the presence of PPB

The hypothesis about the possible correlation between the number of cracks, their length and the presence of carbides and other precipitates at PPBs found a further confirmation referring back to **Figure 3**. As can be observed, signs of corrosion are eliminated after removing a 100 µm thickness of overstock, but PPBs are still present. This partially improves mechanical properties (yielding and bending strengths), but ductility is still limited because PPBs act as preferential sites for secondary cracks nucleation. Only removing 500 µm of overstock allows to eliminate both damages due to corrosion and PPBs and the behavior of bulk superalloy is then reached.

5 Conclusions

The purpose of this research work was to investigate the influence of the leaching process, used to remove the capsule after HIP. More precisely, samples with different finishing condition were bending tested in order to identify the correct overstock material. The overstock material is actually composed by two distinct parts i.e. the corroded layer and the diffusional layer formed between the superalloy powders and the steel capsule during HIP. It was found that the acid leaching process strongly influences the first layers of the superalloy due to the corrosion. The leaching solution chemically attacks the superalloy up to the intense carbide precipitation zone. The bending tests show a progressive enhancement of the mechanical properties as thicker layers of material are removed. More precisely it can be concluded that the effects of the corrosion can be eliminated by removing the first 100 µm of material. Nevertheless, the influence of PPBs must be added to the effects of corrosion. In fact, even by removing the corroded layer, elongation at break values do not reach those of the bulk material. PPBs and carbides, in fact, acts as stress concentration sites and are detrimental for mechanical properties. Therefore, to entirely suppress the effects of corrosion and PPBs, a layer of 500 µm below the leaching surface must be removed.

Acknowledgment

The authors would like to thank the European Committee for their support on the FP7 Clean Sky Joint Undertaking project “HiGh spEed TuRbinE cAsing produced by powDer HIP technologY (GETREADY)”, Grant Agreement No: 641594

Reference

Adler, T.A., Aylor, D., Bray, A., 2003. Corrosion: Fundamentals, Testing, and Protection ASM INTERNATIONAL ® Publication Information and Contributors. https://doi.org/10.1021/la200122x

ASTM E290-14, Standard Test Methods for Bend Testing of Material for Ductility, 2014.

Atkinson, H.V., and Davies, S., 2000. Fundamental aspects of hot isostatic pressing: an overview. Phys. Metall. Mater. Trans. 31, 2981–3000.

Aubin, C., Davidson, J.H., Trottier, J.P., 1980. The Influence Of Powder Particle Surface Composition On the properties of a Nickel-based superalloy produced by hot isostatic pressing. superalloys 345–354.

Baccino, R., Moret, F., Pellerin, F., Guichard, D., Raisson, G., 2000. High performance and high complexity net shape parts for gas turbines: the ISOPREC® powder metallurgy process. Mater. Des. 21, 345–350. https://doi.org/10.1016/S0261-3069(99)00093-X

Bampton, C., Goodin, W., Daam, T. Van, Creeger, G., James, S., 2005. Net shape HIP powder metallurgy components for rocket engines. HIP05 Proc.

Bassini, E., Marchese, G., Cattano, G., Lombardi, M., Biamino, S., Ugues, D., Vallillo, G., Picqué, B., 2017a. Influence of solutioning on microstructure and hardness of hot isostatically pressed Astroloy. J. Alloys Compd. 723, 1082–1090. https://doi.org/10.1016/j.jallcom.2017.06.332

Bassini, E., Vola, V., Lorusso, M., Ghisleni, R., Lombardi, M., Biamino, S., Ugues, D., Vallillo, G., Picqué, B., 2017b. Net shape HIPping of Ni-superalloy: Study of the interface between the capsule and the alloy. Mater. Sci. Eng. A 695. https://doi.org/10.1016/j.msea.2017.04.016

Bassini, E., Vola, V., Lorusso, M., Ghisleni, R., Lombardi, M., Biamino, S., Ugues, D., Vallillo, G., Picqué, B., 2017. Net shape HIPping of Ni-superalloy_ Study of the interface between the capsule and the alloy. Mater. Sci. Eng. A 695, 55–65. https://doi.org/10.1016/j.msea.2017.04.016

Bergmann, C., 1990. HIP quenching in 2000 bar argon gas. Met. Powder Rep. 45, 669–672. https://doi.org/10.1016/0026-0657(90)90933-8

Broeckmann, C., 2012. Hot isostatic pressing of near net shape components – process fundamentals and future challenges. Powder Metall. 55, 176–179. https://doi.org/doi:10.1179/0032589912Z.00000000063

Cai, C., Song, B., Xue, P., Wei, Q., Wu, J.M., Li, W., Shi, Y., 2016. Effect of hot isostatic pressing procedure on performance of Ti6Al4V: Surface qualities, microstructure and mechanical properties. J. Alloys Compd. 686, 55–63. https://doi.org/10.1016/j.jallcom.2016.05.280

Davidson, A., Zhang, K., Yuan, W., Mei, J., Hurley, P., Bache, M.R., Loretto, M.H., Voice, W.E., Wu, X.H., 2006. Influence of surface layer on properties of hipped Ti–6Al–4V. Mater. Sci. Technol. 22, 553–560. https://doi.org/10.1179/174328406X84085

Donachie, M.J., Donachie, S.J., 2002. Selection of Superalloys for Design, in: Kutz, M. (Ed.), Handbook of Materials Selection. John Wiley & Sons, Inc., New York, pp. 293–334. https://doi.org/10.1002/9780470172551.ch10

Donachie, M.J., Donachie, S.J., 2002. Superalloys: A Technical Guide, 2nd Editio. ed. ASM International.

Eklund, A., Ahlfors, M., 2018. Heat treatment of PM parts by Hot Isostatic Pressing. Met. Powder Rep. 73, 163–169. https://doi.org/10.1016/j.mprp.2018.01.001

ElRakayby, H., Kim, K.T., 2018. Effect of glass container encapsulation on deformation and densification behavior of metal powders during hot isostatic pressing. Int. J. Mater. Form. 11, 517–525. https://doi.org/10.1007/s12289-017-1361-8

Friend, W.Z., 1980. Corrosion of nickel and nickel-base alloys. Wiley.

Geddes, B., Leon, H., Huang, X., 2010. Superalloys, Alloying and Performance, 1st Ed. ed.

Gessinger, G.H., 1984. Powder Metallurgy of Superalloys. Butterworth & Co.

Go, X., Echeberria, J., 2003. Microstructure and mechanical properties of carbon steel A210 Á superalloy Sanicro 28 bimetallic tubes 348, 180–191.

Hjorth, C.G., 2007. HIP Powder Metal Near-Net Shapes for Demanding Environment and Applications. J. Iron Steel Res. Int. 14, 121–125. https://doi.org/10.1016/S1006-706X(08)60064-3

López, B., Gutiérrez, I., Urcola, J.J., 1996. Microstructural analysis of steel-nickel alloy clad interfaces. Mater. Sci. Technol. 12, 45–55.

Popoolaa, A.P.I., Oluwasegun, K.M., Olorunniwo, O.E., Atanda, P.O., Aigbodion, V.S., 2016. Thermal and mechanical effect during rapid heating of astroloy for improving structural integrity. J. Alloys Compd. 666, 482–492. https://doi.org/10.1016/j.jallcom.2016.01.012

Qiu, C.L., Attallah, M.M., Wu, X.H., Andrews, P., 2013. Influence of hot isostatic pressing temperature on microstructure and tensile properties of a nickel-based superalloy powder. Mater. Sci. Eng. A 564, 176–185. https://doi.org/10.1016/j.msea.2012.11.084

Raisson, G., 2008. Evolution of PM nickel base superalloy processes and products. Powder Metall. 51, 10–13. https://doi.org/10.1179/174329008X286631

Raisson, G., Guédou, J.Y., Guichard, D., Rongvaux, J.M., 2011. Production of Net-Shape Static Parts by Direct HIPing of Nickel Base Superalloy Prealloyed Powders. Adv. Mater. Res. 278, 277–282. https://doi.org/10.4028/www.scientific.net/AMR.278.277

Reed, R.C., 2006. The Superalloys, Fundamentals and Applications, 1st Ed. ed. Cambridge University press, Cambridge.

Rolls-Royce, 1996. The jet engine.

Scherillo, F., Aprea, P., Astarita, A., Scherillo, A., Testani, C., Squillace, A., 2015. On the Interface Generated by Hot Isostatic Pressing Compaction Process Between an AISI 304 Container and the Ti6Al4V Powders. Metall. Mater. Trans. A Phys. Metall. Mater. Sci. 46, 2376–2379. https://doi.org/10.1007/s11661-015-2868-6

Wisniewski, A., Beddoes, J., 2009. Influence of grain-boundary morphology on creep of a wrought Ni-base superalloy. Mater. Sci. Eng. A 510–511, 266–272. https://doi.org/10.1016/j.msea.2008.04.130

Zhang, K., Mei, J., Wain, N., Wu, X., 2010. Effect of hot-isostatic-pressing parameters on the microstructure and properties of powder Ti-6Al-4V hot-isostatically-pressed samples. Metall. Mater. Trans. A Phys. Metall. Mater. Sci. 41, 1033–1045. https://doi.org/10.1007/s11661-009-0149-y